Letter Vol. 43, No. 4 / 15 February 2018 / Optics Letters 883

Recovering a hidden polarization by ghost polarimetry

PATRICK JANASSEK, SÉBASTIEN BLUMENSTEIN, AND WOLFGANG ELSÄßER*

Institute of Applied Physics, Technische Universität Darmstadt, Schlossgartenstrasse 7, 64289 Darmstadt, Germany
**Corresponding author: elsaesser@physik.tu-darmstadt.de*

Received 13 November 2017; accepted 22 December 2017; posted 9 January 2018 (Doc. ID 313224); published 14 February 2018

By exploiting polarization correlations of light from a broadband fiber-based amplified spontaneous emission source we succeed in reconstructing a hidden polarization in a ghost polarimetry experiment in close analogy to ghost imaging and ghost spectroscopy. Thereby, an original linear polarization state in the object arm of a Mach–Zehnder interferometer configuration which has been camouflaged by a subsequent depolarizer is recovered by correlating it with light from a reference beam. The variation of a linear polarizer placed inside the reference beam results in a Malus law type second-order intensity correlation with high contrast, thus measuring a ghost polarigram.

OCIS codes: (120.5410) Polarimetry; (270.5290) Photon statistics; (260.5430) Polarization; (030.1640) Coherence.

https://doi.org/10.1364/OL.43.000883

Ghost imaging (GI) modalities [1–5] in the framework of spatial ghost imaging [6–8], temporal ghost imaging [9–12], and ghost spectroscopy (GS) [13,14] are modalities exploiting photon correlations in the spatial, temporal, or spectral domains, respectively. The correlation can either be realized in the quantum domain with entangled photons [6,13] or in the classical domain by exploiting photon bunching of thermal light sources [7,15,16]. Particularly interesting are amplified spontaneous emission (ASE) sources as semiconductor-based superluminescent diodes [17–21] or fiber-based amplifiers. The successful implementation of this ASE concepts in ghost imaging modalities has been demonstrated recently [18–21]. Though ghost imaging was successfully introduced already in 1995 [6], there is still a vivid and perpetual discussion on the superiority and the unique advantages of ghost modalities exploiting photon correlations [22] against non-correlation methods accompanied by the search for specific applications which demonstrate these benefits [23]. In ghost imaging, the superiority in turbulent or challenging environments introduced into the object arm has been suggested and already demonstrated [24–28]; in GS such a proof is yet awaiting. Here in this Letter, we move into the polarization domain [29]. Polarization is an important variable in quantum communication schemes and having a high fidelity in the degree of polarization (DoP) is ultimately requested for any successful communication scheme [30]. Either intentional attacks or more natural depolarization mechanisms as in free-space or in fibers with polarization mode dispersion ultimately limit the performance. Therefore, there is the interesting question if after destruction or camouflage of an original state of polarization thus making it invisible to direct detection schemes, this camouflaged state of polarization can be eventually retrieved by intensity correlation techniques in the polarization domain, i.e., ghost polarimetry (GP).

Here, we demonstrate that a linear state of polarization prepared in the object arm out of unpolarized light emitted from a broadband fiber-based ASE source and subsequently camouflaged by a depolarizer can indeed be successfully recovered by correlating it with linearly polarized light from the reference arm. By varying the polarization angle of the reference arm polarizer a Malus law dependence of the second-order correlation coefficient is found exhibiting the well-known $\cos^2(\theta)$ dependence with high fidelity. These second-order intensity correlations as a function of polarizer angle in the reference arm—in the framework of Malus law—are the equivalent of spatial point-to-point correlations in GI or spectral lambda-lambda correlations in GS [21]. This allows us to understand the functionality of a ghost polarimetry experiment.

Experimental Setup: We used a standard classical ghost imaging setup, as shown in Fig. 1. A beam splitter divides the unpolarized amplified spontaneous emission light with a central wavelength at 1534 nm from an erbium-doped fiber amplifier (EDFA) into a reference arm and an object arm, respectively. Behind the beam splitter a linear polarizer with fixed polarization (θ_{obj}) and eventually a depolarizer (DEP) are introduced into the object arm whereas a rotatable polarizer (θ_{ref}) is placed in the reference arm. The light of each arm is individually coupled into polarization-controllable fibers and after superposition by a fiber coupler is directed to a photomultiplier tube (PMT) operated in two-photon absorption (TPA) mode [31]. Together with a motorized delay stage (delay time τ) in the object arm this allows for determining the TPA interferogram in terms of the TPA-PMT photocurrent $I_{\mathrm{TPA}}(\tau) = \mathrm{function}(G^{(2)}(\tau))$ [31] from which the second-order intensity correlation $G^{(2)}(\tau)$ between the object and reference arms is evaluated [31]:

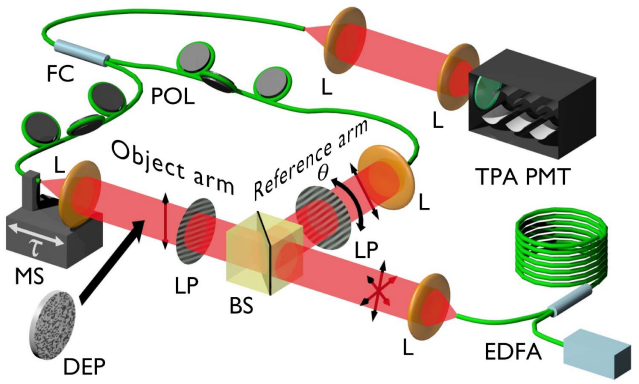

Fig. 1. Schematic diagram of the ghost polarimetry experiment. The setup comprises the fiber-based ASE light source emitting at 1534 nm (EDFA), collimating and focusing achromatic lenses (L), a non-polarizing beam splitter (BS), a rotatable linear polarizer (LP) in the reference arm followed by a fiber coupling unit, a fixed linear polarizer (LP) in the object arm with eventually a subsequently following liquid crystal depolarizer (DEP), again followed by a fiber coupling unit, a single-mode fiber-based combiner (FC), a motorized linear translation stage (MS), polarization controlling elements (POL), and the PMT (Hamamatsu H7421-40) operated in two-photon absorption (TPA) mode (TPA-PMT) including a long-pass filter (Schott RG1000) preventing visible light from entering the detector.

$$G^{(2)}(\tau,\theta_{\mathrm{obj}},\theta_{\mathrm{ref}}) = \langle I_{\mathrm{ref}}(t,\theta_{\mathrm{ref}})I_{\mathrm{obj}}(t+\tau,\theta_{\mathrm{obj}})\rangle_t. \quad (1)$$

Normalization of $G^{(2)}(\tau)$ by dividing by the $G^{(2)}$ value at very large delay $\tau \gg \tau_c$, with τ_c as the first-order coherence time yields finally the normalized second-order intensity correlation coefficient $g^{(2)}(\tau) = G^{(2)}(\tau)/G^{(2)}(\tau \gg \tau_c)$ [31].

Results and Discussion: Prior to the ghost polarimetry experiments we checked for correct intensity dynamics operation of the interferometer and the detection scheme as well as for polarization (in)sensitivity of the correlation measurements. For verifying the linear operation of the correlation interferometer, we varied the intensity ratio $I_{\mathrm{obj}}/I_{\mathrm{ref}}$ between the object and reference arms by introducing a variable neutral density filter into the reference arm and keeping the intensity I_{obj} constant. For intensity ratios $I_{\mathrm{obj}}/I_{\mathrm{ref}}$ between 10^{-2} and 1, we found $g^{(2)}(\tau)$ values equal to 1.46 ± 0.04 and 2.03 ± 0.09 when injecting unpolarized light directly from the EDFA source with a degree of polarization DoP = 0.05 and fully linearly polarized (DoP = 1.0) light, respectively. The DoP values had been both obtained by a Stokes parameter analysis [32]. These central correlation coefficient values $g^{(2)}(\tau = 0)$ are in accordance with theoretical values of $g^{(2)}(\tau = 0, \mathrm{DoP}) = 3/2 + 1/2 \cdot (\mathrm{DoP})^2$ resulting in expected values of $g^{(2)}(\tau = 0)_{\mathrm{pol}}$ of 2.0 and $g^{(2)}(\tau = 0)_{\mathrm{unpol}}$ of 1.5, respectively [33]. We could even observe these characteristic $g^{(2)}(\tau = 0)$ values for intensity ratios $I_{\mathrm{obj}}/I_{\mathrm{ref}}$ down to 10^{-4}, however with increased error bars for $g^{(2)}(\tau = 0)$ of up to ± 0.2.

We then verified the proper TPA signal of the PMT in respect of the polarization constellations of the light in the two arms, subsequently impinging on the TPA-PMT where the fiber polarization controllers realized various linear polarization states between 90° (vertical V) and 0° (horizontal H). Figure 2 (top) shows the TPA interferograms, i.e., the

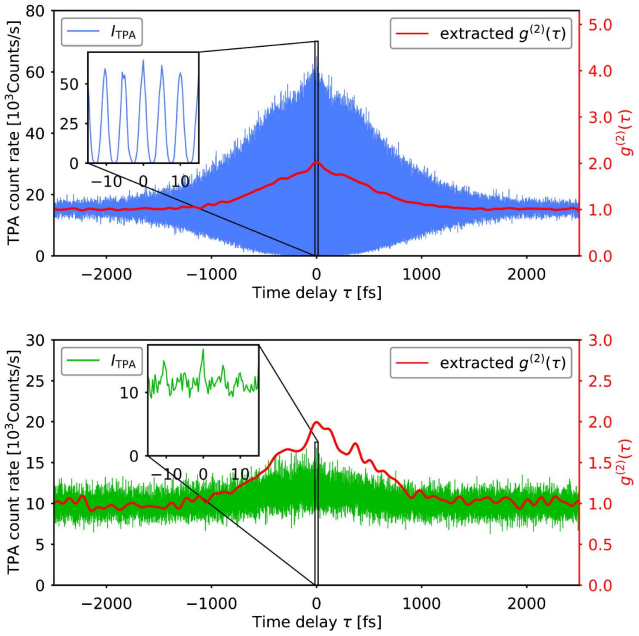

Fig. 2. Measured interferometer signal in terms of second-order TPA current of the TPA-PMT for light with parallel polarization (H-H) in both arms (top, in blue) and for light with orthogonal polarization (V-H) in the reference and object arms (bottom, in green). The insets show in both cases a time-scale enlarged part. The curves in red (right scale) inserted into the interferograms represent the normalized second-order correlation coefficient $g^{(2)}(\tau)$.

photocurrent of the TPA-PMT for the case of parallel polarization of the reference and object arms and Fig. 2 (bottom) depicts the results for the case of the polarizations of both arms being orthogonal to each other, respectively. The latter realization of these polarization constellations was performed by selecting parallel polarizations in both arms and using the polarization-controlling element in the object arm to rotate this linear polarization by 90°. According to the inference laws of Fresnel and Arago, first-order interference is only observed for parallel polarization [34,35]. The insets with an enlargement of both interferograms show this clearly where only very small first-order interference fringes visible as small peaks are present for orthogonal polarization (bottom part of Fig. 2). Low-pass filtering both interferograms assuming the same cutoff frequency yields the low-pass filtered TPA-PMT photocurrent $I_{\mathrm{TPA}}(\tau)$ from which together with Eq. (1) and after normalization of the second-order correlation coefficients $g^{(2)}(\tau)$ can be calculated, which are depicted as red curves for both cases in Fig. 2. The important outcome is that even though the interferogram traces are smaller for orthogonal polarization than for parallel polarization, the central second-order correlation coefficient at $\tau = 0$, i.e., $g^{(2)}(\tau = 0)$ amounts to $g^{(2)}_{\mathrm{para}}(\tau = 0) = 2.00 \pm 0.04$ and $g^{(2)}_{\mathrm{orth}}(\tau = 0) = 2.03 \pm 0.03$, respectively. Therefore, from this point onwards we do not take care about modifications of the polarization in the fibers because it has no effect on the $g^{(2)}$ values. These results of the independency of the central second-order correlation values on the polarization in the interferometer arms [36,37] and thus the preservation of photon bunching with high degree assure the functionality of our GP scheme for retrieving a hidden or really camouflaged

polarization. When having a *per se* unknown or hidden polarization we can absolutely not establish in the subsequent experiments a polarization reference in the detection branch when searching to recover it.

We then place a linear polarizer at 90° (V-polarization) in the object arm. A linear polarizer in the reference arm is rotated from 0° to 180° in steps of 10° and we measured $g^{(2)}(\tau,\theta)$. Figure 3 shows in red the result of these polarization-angle correlations of the ghost polarimetry experiment in terms of $g^{(2)}(\tau,\theta)$ as a function of the analyzer angle θ. Also shown are results of a standard direct intensity measurement in green performed with a germanium photodiode directly behind the polarization analyzer, which has been placed behind the object arm polarizer. One can observe second-order correlation coefficients between ($g^{(2)} \approx 1.1$) and ($g^{(2)} \approx 2.0$). This nearly full-scale variation of the normalized polarization-polarization correlation coefficient $g^{(2)}$ values from no correlation ($g^{(2)} \approx 1$) to a thermal photon-bunching behavior ($g^{(2)} \approx 2$) reveals a remarkable degree of polarization-dependent intensity correlations of the emitted light from the ASE source. A $\cos^2$ fit to the $g^{(2)}(\theta_{\mathrm{ref}})$-data traces accurately the experimental values of the direct polarization measurements. Both curves exhibit a Malus law dependence according to $I_{\mathrm{Malus}}(\theta) = I_0 \cdot \cos^2(\theta - \theta_0)$ and $g^{(2)}(\tau = 0,\theta) \propto \cos^2(\theta - \theta_0)$, respectively, with $\theta_0 = 91.1 \pm 0.04°$ for the direct polarization measurement case and with $\theta_0 = 87.1 \pm 0.6°$ for the second-order correlation case. Thus, both results are reflecting the original 90° polarization with high contrast or fidelity.

We then applied a polarization scrambling procedure, some type of polarization turbulence onto the linear polarization state in the object arm by introducing a liquid crystal DEP into the beam behind the polarizer. The polarization results are now depicted in Fig. 4. Figure 4 shows in green again a direct standard measurement of the intensity $I(\theta)$ with a rotated analyzer. The direct measurement no longer shows any reminiscence of Malus law, i.e., absolutely no linear polarization. Even when enlarging the results (top of Fig. 4) no conclusion on the correct original linear polarization at 90° can be drawn and only a weak modulation with $I_{\mathrm{max}} = 1.000$ and $I_{\mathrm{min}} = 0.992$ can be recognized, however displaced from 90° (V). These I_{max} and I_{min} values result in a contrast $C = (I_{\mathrm{max}} - I_{\mathrm{min}})/(I_{\mathrm{max}} + I_{\mathrm{min}})$ of

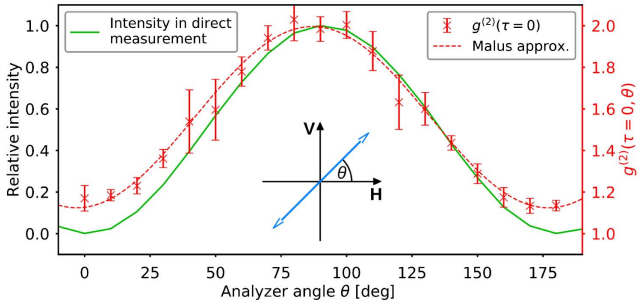

Fig. 3. Measured polarization-polarization second-order intensity correlations of light emitted by the ASE light source in red (right scale) and a direct polarization measurement with a polarizer and an analyzer as a function of polarization angle θ in green (left scale). Both curves are fitted in terms of a Malus' law $\cos^2(\theta)$ dependence. The error bars in the correlation measurements correspond to the variance of a set of five measurements. The inset in the middle shows the polarization angle geometry.

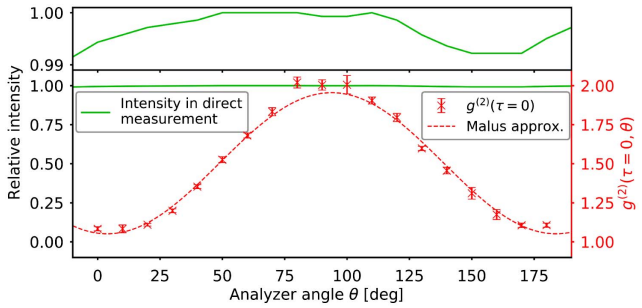

Fig. 4. Experimental results of the ghost polarimetry experiment: the data points (red crosses, right scale) represent the second-order polarization correlation values [Eq. (1)], thus the ghost polarigram measured according to Fig. 1, whereas the green data (left scale) depict a direct polarization measurement with a polarizer and an analyzer at a polarization angle θ. The error bars in the correlation measurements correspond to the variance of a set of five measurements. The top picture shows intensity enlarged results for the standard direct measurement of the angle dependence for the camouflaged polarization state.

$C = 0.004$. In contrast, the ghost polarimetry correlation results, i.e., $g^{(2)}(\tau,\theta)$ shown in red in Fig. 4, clearly reflect the original linear polarization state with nearly unobstructed fidelity with $g^{(2)}_{\mathrm{max}} = 1.955$ and $g^{(2)}_{\mathrm{min}} = 1.051$. From these $g^{(2)}$ values a contrast $C = (g^{(2)}_{\mathrm{max}} - 1 - (g^{(2)}_{\mathrm{min}} - 1))/(g^{(2)}_{\mathrm{max}} - 1 + g^{(2)}_{\mathrm{min}} - 1)$ with $C = 0.90 \pm 0.02$ is obtained (here, we used a contrast definition considering the offset of $g^{(2)}$ from unity). A fit to the second-order correlation results in terms of a Malus law yields $\theta_0 = 93.8° \pm 0.7°$ and thus a very good agreement with the original Malus law (c.f. Fig. 3), which exhibits the linear polarization at 90°. These ghost polarimetry results obtained in the framework of polarization correlations clearly demonstrate that our realized classical GP experiment exploiting polarization-polarization correlations of correlated classical photons enables the recovery of a hidden polarization, thus assuring the functionality of GP.

We would like now to discuss the performed GP experiments in the framework of analogies to GI and GS [14,21]. In GI spatially broadband light illuminates the amplitude object and is detected with a non-resolving bucked detector. The spatial resolution is performed within the reference arm and then both intensities are correlated with each other [21]. The same analogy holds for classical ghost spectroscopy where a spectrally broadband source exhibiting spectral correlations is exploited [14]. The setup can be considered as replacing the spatial variables by spectral variables and the spatial resolution of the scanning aperture in the reference arm by a grating or a tunable filter.

Here in GP, we illuminate with polarization-broad light, i.e., unpolarized light, place a polarization object into the object arm, and detect the reference arm light with polarization resolution. The polarizer in the reference projects one polarization out of the unpolarized reference beam and subsequently the correlations between both beams are determined. A remarkable difference in the three techniques lies in the fact that spatial coordinates and wavelengths are scalars decaying quite fast on the corresponding spatial scale as point-to-point correlations or on the spectral scale as lambda-lambda correlations in GI and

GS, respectively, whereas in GP the polarization-polarization correlations are governed by the vector nature of the polarization, thus resulting in the rather smooth, continuous correlation according to Malus's law. Our GP results show that polarization intensity correlations can be measured and exploited for recovering a polarization state of a light beam that has not been polarization-resolved. It can be interpreted as a prerequisite of recently proposed ghost ellipsometry schemes [38,39] that rely on the change of polarization of light impinging on a sample within a "ghost" modality, i.e., the detection of the final polarization state by a polarization-correlated reference beam via polarization-polarization intensity correlations.

Finally, we would like to conclude with a suggestion for exploiting GP in a real-world application. This analogy of GP to ghost imaging and ghost spectroscopy could be exploited in a real-world ghost polarimetry experiment, a saccharimetry metrology experiment [40] in strongly polarization disturbing media [41], as, e.g., grape most or pharmaceutical solution with scatterers as, e.g., lipofundin where always a clearing filtering procedure has to be requested before measuring the sugar content. Placing the scattering sugar or pharmaceutical solution within the object beam should allow for determining the polarization rotation angle by the sugar, irrespective of the scattering.

Summary: In conclusion, we have demonstrated experimentally that a linear polarization state scrambled and thus camouflaged in the object arm of a ghost polarimetry experiment can be reconstructed by correlation of the object arm light with polarization-resolved light of the reference arm, thus the ghost polarigram. This demonstrated GP modality is in close analogy to GI and GS. An interesting application for the determination of sugar content or other enantiomorphic substances changing the handedness in strongly scattering media has been suggested and discussed. Furthermore, we suggest the extension of this described GP recovery scheme on other polarization states.

Funding. Deutsche Forschungsgemeinschaft (DFG) (EL105/21); Deutscher Akademischer Austauschdienst (DAAD) (Breakthroughs in Ghost Imaging).

Acknowledgment. We thank Prof. A. T. Friberg and Prof. G. Genty for discussions about GI modalities.

REFERENCES AND NOTE

1. D. S. Simon, G. Jaeger, and A. V. Sergienko, *Quantum Metrology, Imaging, and Communication* (Springer, 2017).
2. J. H. Shapiro and R. W. Boyd, Quantum Inf. Process. **11**, 949 (2012).
3. M. Padgett, R. Aspden, G. Gibson, M. Edgar, and G. Spalding, Opt. Photon. News **27**(10), 38 (2016).
4. B. I. Erkmen and J. H. Shapiro, Adv. Opt. Photon. **2**, 405 (2010).
5. M. J. Padgett and R. W. Boyd, Philos. Trans. R. Soc. London Ser. A **375**, 20160233 (2017).
6. T. B. Pittman, Y. H. Shih, D. V. Strekalov, and A. V. Sergienko, Phys. Rev. A **52**, R3429 (1995).
7. R. S. Bennink, S. J. Bentley, and R. W. Boyd, Phys. Rev. Lett. **89**, 113601 (2002).
8. D. Zhang, Y.-H. Zhai, L.-A. Wu, and X.-H. Chen, Opt. Lett. **30**, 2354 (2005).
9. P. Ryczkowski, M. Barbier, A. T. Friberg, J. M. Dudley, and G. Genty, Nat. Photonics **10**, 167 (2016).
10. F. Devaux, P.-A. Moreau, S. Denis, and E. Lantz, Optica **3**, 698 (2016).
11. F. Devaux, K. P. Huy, S. Denis, E. Lantz, and P.-A. Moreau, J. Opt. **19**, 024001 (2017).
12. S. Denis, P.-A. Moreau, F. Devaux, and E. Lantz, J. Opt. **19**, 034002 (2017).
13. G. Scarcelli, A. Valencia, S. Gompers, and Y. Shih, Appl. Phys. Lett. **83**, 5560 (2003).
14. P. Janassek, S. Blumenstein, and W. Elsäßer, Phys. Rev. Appl. **9**, (2018).
15. F. Ferri, D. Magatti, A. Gatti, M. Bache, E. Brambilla, and L. A. Lugiato, Phys. Rev. Lett. **94**, 183602 (2005).
16. A. Gatti, M. Bache, D. Magatti, E. Brambilla, F. Ferri, and L. A. Lugiato, J. Mod. Opt. **53**, 739 (2006).
17. We note that from a semiconductor technology point of view a superluminescent diode (SLD) is equivalent to a semiconductor optical amplifier (SOA) used in telecommunication applications.
18. S. Kuhn, S. Hartmann, and W. Elsäßer, Opt. Lett. **41**, 2863 (2016).
19. S. Hartmann, S. Kuhn, and W. Elsäßer, Appl. Opt. **55**, 7972 (2016).
20. S. Hartmann, A. Molitor, and W. Elsäßer, Opt. Lett. **40**, 5770 (2015).
21. S. Hartmann and W. Elsäßer, Sci. Rep. **7**, 41866 (2017).
22. G. Brida, M. V. Chekhova, G. A. Fornaro, M. Genovese, E. D. Lopaeva, and I. R. Berchera, Phys. Rev. A **83**, 063807 (2011).
23. M. Genovese, J. Opt. **18**, 073002 (2016).
24. R. E. Meyers, K. S. Deacon, and Y. Shih, Appl. Phys. Lett. **98**, 111115 (2011).
25. R. E. Meyers, K. S. Deacon, and Y. Shih, Appl. Phys. Lett. **100**, 131114 (2012).
26. A. Meda, A. Caprile, A. Avella, I. R. Berchera, I. Degiovanni, A. Magni, and M. Genovese, Appl. Phys. Lett. **106**, 262405 (2015).
27. M. Bina, D. Magatti, M. Molteni, A. Gatti, L. A. Lugiato, and F. Ferri, Phys. Rev. Lett. **110**, 083901 (2013).
28. L. A. Lugiato, Istituto Lombardo (Rend. Scienze) **147**, 139 (2013).
29. H. Kellog, T. Setälä, A. T. Friberg, and T. Shirai, J. Opt. **16**, 055702 (2014).
30. A. Sit, F. Bouchard, R. Fickler, J. Gagnon-Bischoff, H. Larocque, K. Heshami, D. Elser, C. Peuntinger, K. Günthner, B. Heim, C. Marquardt, G. Leuchs, R. W. Boyd, and E. Karimi, Optica **4**, 1006 (2017).
31. F. Boitier, A. Godard, E. Rosencher, and C. Fabre, Nat. Phys. **5**, 267 (2009).
32. E. Collett, *Polarized Light: Fundamentals and Applications* (Marcel Dekker, 1993).
33. R. Loudon, *The Quantum Theory of Light*, 2nd ed. (Oxford Clarendon, 1995).
34. M. Mujat, A. Dogariu, and E. Wolf, J. Opt. Soc. Am. **21**, 2414 (2004).
35. E. Collett, Am. J. Phys. **39**, 1483 (1971).
36. A. Nevet, T. Michaeli, and M. Orenstein, J. Opt. Soc. Am. B **30**, 258 (2013).
37. A. Shevchenko, M. Roussey, A. T. Friberg, and T. Setälä, Optica **4**, 64 (2017).
38. A. Hannonen, A. T. Friberg, and T. Setälä, Opt. Lett. **41**, 4943 (2016).
39. A. Hannonen, A. T. Friberg, and T. Setälä, J. Opt. Soc. Am. A. **34**, 1360 (2017).
40. W. R. Brode, J. Opt. Soc. Am. **41**, 987 (1951).
41. L.-H. Lin, Y.-L. Lo, C.-C. Liao, and J.-X. Lin, Appl. Opt. **54**, 10425 (2015).